# EFFECT OF THE LASER POLARIZATION ON ELECTRON ACCELERATION IN CARBON NANOTUBE TARGETS*

B.S. Nunes†, N.D. Vieira Junior, R.E. Samad, Nuclear and Energy Research Institute, São Paulo, Brazil
A. Bonatto, M.S. Alva-Sánchez, Universidade Federal de Ciências da Saúde de Porto Alegre, Porto Alegre, Brazil
B. Lei, C. Bonţoiu, University of Liverpool, Liverpool, United Kingdom
G. Xia, University of Manchester, Manchester, United Kingdom
J. Resta-López, Instituto Universitario de Ciencia de los Materiales, Valencia, Spain

*Abstract*

Structured carbon-nanotube targets can be used as a medium for accelerating self-injected electrons within a laser-driven wakefield bubble, analogous to blowout laser wakefield acceleration (LWFA) in gaseous plasmas. A previous numerical work demonstrated this behavior using a three-cycle, 800 nm, circularly polarized laser pulse with a peak power of 35.5 TW. Here, we compare electron beam properties for linearly and circularly polarized pulses interacting with a similar target. We found that circular polarization increases the charge of electrons above 20 MeV by approximately 10%, while average energy, energy spread, emittance, and divergence remain comparable between the two polarization states.

## INTRODUCTION

Over the past few decades, plasma-based accelerators [1, 2] have emerged as a promising approach for electron acceleration using either ultraintense laser pulses—known as laser wakefield acceleration (LWFA) [4]—or charged particle beams, called beam-driven wakefield acceleration (PWFA) [3, 5]. In these schemes, the driver propagates through an ionized gas, typically generated by gas jets or capillary discharge cells, exciting large-amplitude wakefields by perturbing the local electron density. These wakefields can sustain accelerating gradients on the order of 100 GeV/m, enabling the production of high-quality electron bunches for a wide range of applications, including medical radioisotope production [6], radiotherapy [7], industrial applications [8], and high-energy physics research [9, 10].

Because the accelerating gradient scales with plasma density, substantially higher fields may be achieved using solid-state plasmas, whose electron densities ($10^{22}$–$10^{24}$ cm$^{-3}$) are approximately five orders of magnitude greater than those of conventional gaseous plasmas. In principle, this increase could enable accelerating gradients approaching the TeV/m regime. This concept was demonstrated in numerical studies by Bonţoiu et al. [11, 12], where particle-in-cell (PIC) simulations showed that solid-state targets composed of carbon nanotube (CNT) bundles can serve as an effective medium for accelerating self-injected electrons within a laser-driven wakefield bubble, analogous to the blowout regime of LWFA in gaseous plasmas.

In a recent study [12], Bonţoiu et al. employed the PIConGPU code [13] to demonstrate that a three-cycle, 800 nm, circularly polarized laser pulse with a peak power of 35.5 TW can generate a relativistic electron bunch in a CNT bundle target. Motivated by those results, we performed analogous fully three-dimensional PIC simulations using the WarpX v. 25.10 code [14]. Here, we directly compare the electron beam properties obtained with linearly and circularly polarized laser pulses interacting with the same CNT bundle target, aiming to assess the influence of the laser polarization on the acceleration process.

## THE MODEL

The 3D-WarpX simulations were carried out on the SDumont cluster, using 16 NVIDIA Volta V100 GPUs (32 GB each). The physical system consists of an 800 nm wavelength laser pulse propagating along the $z$-axis through a CNT bundle target whose longitudinal direction is aligned with the laser propagation axis. The laser is modeled by a few-cycle Gaussian temporal and transverse profile [15]. Six simulations were carried out, combining two laser polarizations (linear along $y$ and circular) and three targets.

The computational domain extends from $-3.5$ μm $\leq z \leq$ 27.5 μm longitudinally and $-3.5$ μm $\leq x, y \leq 3.5$ μm transversely, with $N_{x,y,z} = 1024$ cells in each direction. Each cell is initialized with $N_{\mathrm{PPC}} = 8$ macroparticles ($2 \times 2 \times 2$). The timestep is set to 0.999 CFL, where CFL denotes the Courant–Friedrichs–Lewy stability limit. For the Yee solver, this corresponds to $dt = 15.9$ as. The simulations are run for $N_{\mathrm{step}} = 5250$ time steps. The laser parameters are $a_0 = 21.6$, $\lambda_0 = 800$ nm, $w_0 = 1.5$ μm, pulse duration $\tau = 2.67$ fs (FWHM in intensity), peak intensity $I_0 = 10^{21}$ W/cm$^2$, and pulse energy $E = 100$ mJ.

The target geometry reproduces that described in Ref. [12], although the present simulations employ higher spatial resolution and a larger number of particles per cell. The target

* THIS STUDY WAS FINANCED IN PART BY THE CONSELHO NACIONAL DE DESENVOLVIMENTO CIENTIFICO E TECNOLÓGICO (CNPQ, GRANTS 405143/2021-4 AND 140941/2023-1), BY THE FUNDAÇÃO DE AMPARO À PESQUISA DO ESTADO DO RIO GRANDE DO SUL (FAPERGS, GRANT 24/2551-0001552-3), AND BY THE COORDENAÇÃO DE APERFEIÇOAMENTO DE PESSOAL DE NÍVEL SUPERIOR - BRASIL (CAPES) - FINANCE CODE 001.
† brunosnunes@usp.br

consists of CNT bundles modeled as initially neutral solid carbon cylinders with radius $r_b = 12.5$ nm and density $n_b = 10^{22}$ cm$^{-3}$. The bundles are arranged along concentric cylindrical shells that serve as immaterial geometric guides for their spatial distribution. For each shell, the number of bundles and their angular separation are chosen to maintain a constant effective density along the circumference, with positions determined from a random initial phase angle. Three different random seeds generated the bundle distributions, producing three distinct target realizations (targets 1, 2, and 3). Each target was simulated with both linear and circular laser polarizations. This procedure yields an overall effective density [16] of $n_{\text{eff}} = 3 \times 10^{20}$ cm$^{-3}$. A central aperture with inner radius $r_{in} = 0.8$ μm is included to allow propagation of the laser core through the target. Despite representing the same physical system, different postprocessing approaches prevent direct comparison between the results of this work and those reported in Ref. [12]. In the present study, all particles exiting the target whose longitudinal momentum corresponds to kinetic energies above 20 MeV are considered, allowing the analysis to focus on the highest-energy electrons accelerated during the interaction.

## RESULTS

Following the mechanism described in Ref. [12], the laser pulse ionizes the CNT target and drives electrons toward the outer shells of the structure. This leads to a propagating wakefield bubble, similar to those observed in laser wakefield acceleration (LWFA) in gas jets and in hollow-channel plasma acceleration [17], as discussed in previous studies [12, 16]. Electrons are self-injected at the rear of the bubble, where they experience longitudinal electric fields on the order of TV/m.

This process is illustrated in the snapshots two simulations with the same target, shown in Fig. 1 (a–f), which depict an approximately 4 μm-wide wakefield bubble propagating inside the target. The left panels—(a), (c), and (e)—display the longitudinal electric field ($E_z$) at the center of the bubble using a blue–white–red color scale for circular laser polarization, while the right panels show the corresponding field for linear polarization. The wakefield bubble contains an electron bunch whose kinetic energy is represented by a yellow–green color scale, applied only to backtracked electrons that satisfy the selection criteria. These electrons are self-injected at the rear of the bubble and subsequently accelerated. The gray lines indicate the positions of a subset of CNT bundles, which illustrate the target geometry. Black contour lines represent the laser intensity.

Overall, the wakefield structures in the left and right panels are very similar, with only minor discrepancies observed behind the bubble rear in panels (c) and (d), and more noticeably in panels (e) and (f). In the latter case, panel (e) exhibits a stronger positive electric field in the region 12.5 μm $< z <$ 15 μm compared to panel (f). Furthermore, in addition to the field discrepancies, small differences are also observed in the accelerated particles. The left-column

Table 1: Bunch parameters at extraction.

| **Parameter** | **Circular** (avg.± std.) | **Linear** (avg.± std.) |
|---|---|---|
| Charge, $Q$ [pC] | 489 ± 4 | 444 ± 8 |
| Average energy, $\bar{E}$ [MeV] | 38.7 ± 0.1 | 37.3 ± 0.3 |
| Energy spread (RMS), $\sigma_E$ [MeV] | 9.3 ± 0.1 | 8.9 ± 0.1 |
| Avg. accel. gradient, $\bar{A}$ [TeV/m] | 2.58 ± 0.01 | 2.49 ± 0.02 |
| Energy conv. eff., $\eta$ [%] | 18.9 ± 0.2 | 16.6 ± 0.3 |
| Bunch size (FWHM): | | |
| $\Delta z$ [μm] | 0.71 ± 0.01 | 0.79 ± 0.02 |
| $\Delta x$ [μm] | 1.7 ± 0.1 | 1.8 ± 0.1 |
| $\Delta y$ [μm] | 1.7 ± 0.2 | 1.6 ± 0.1 |
| Normalized emittance (RMS): | | |
| $\epsilon_x$ [μm rad] | 2.5 ± 0.1 | 2.6 ± 0.1 |
| $\epsilon_y$ [μm rad] | 2.5 ± 0.1 | 2.4 ± 0.1 |
| Divergence (RMS): | | |
| $\Theta_x$ [mrad] | 77 ± 2 | 75 ± 3 |
| $\Theta_y$ [mrad] | 77 ± 1 | 83 ± 2 |

panels show a small number of particles being accelerated within a weakly defined second wakefield bubble, which is not present in the right-column panels.

The properties of the bunch are shown in Fig. 1(g–n), arranged in two rows, circular polarization on top and linear polarization below, to allow direct visual comparison. All eight panels share the same density color scale. Panels (g,h) and (k,l) present the transverse phase spaces. In the circular case, the beam exhibits divergences up to ∼ 0.4 rad and a slight displacement from the target axis, whereas the linear case shows a more centered distribution with particles preferentially aligned along a nearly diagonal structure.

The longitudinal phase spaces (i,m) indicate bunch lengths of approximately 1 μm for both polarizations; however, the linear case displays a distinct V-shaped feature for particles beyond 17 μm that is absent under circular polarization. The transverse spatial distributions (j,n) further highlight different symmetry properties: circular polarization yields a comparatively homogeneous density, with a mild concentration in the quadrant $x < 0$ μm, $y > 0$ μm, while linear polarization produces a clear asymmetry along the $y$-axis, with a larger fraction of particles located at $y < 0$ μm.

Figure 2 shows the electron energy spectra obtained with circular (blue) and linear (red) laser polarization. Solid lines denote the average over three different CNT targets (each simulated with both polarizations), while shaded regions represent the sample standard deviation. Both spectra extend from the 20 MeV selection threshold to nearly 60 MeV and exhibit a well-defined quasi-monoenergetic peak. The average peak energy is slightly higher for circular polarization (approximately 45 MeV) than for linear polarization (approximately 43 MeV). Although the spectral shapes are very similar, circular polarization consistently produces ∼ 10% increase in total charge compared to the linear case.

Table 1 presents the beam parameters averaged over the three target realizations for each laser polarization. Except

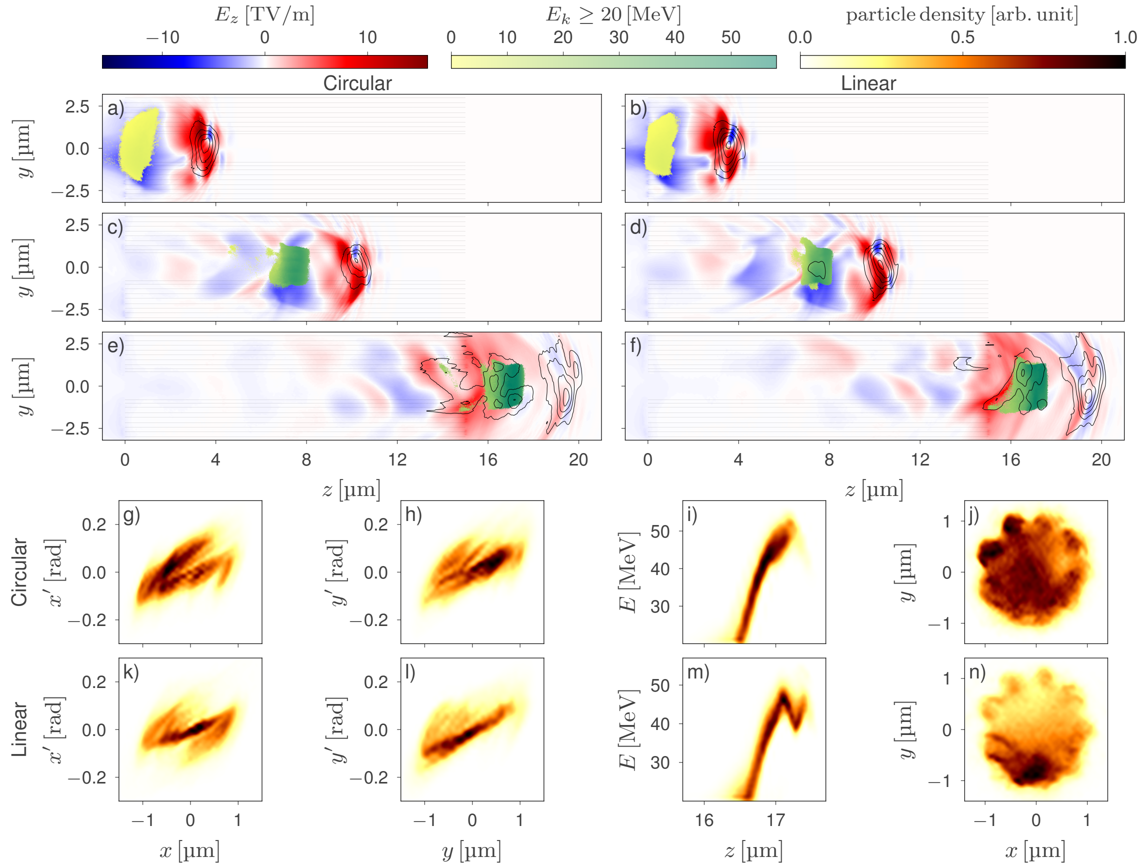


Figure 1: Panels (a–f): propagation stages of the longitudinal electric field ($E_z$, blue–white–red colormap) and accelerated electron macroparticles (yellow–green colormap) in a CNT target with effective density $n_e \simeq 3 \times 10^{20}$ cm$^{-3}$; left column: circular polarization, right: linear. Gray lines: selected CNT bundles; black contours: laser intensity. Panels (g–n): extracted bunch properties—transverse phase spaces (g, h, k, l), longitudinal phase spaces (i, m), and transverse spatial distributions (j, n); upper row: circular polarization, lower: linear.

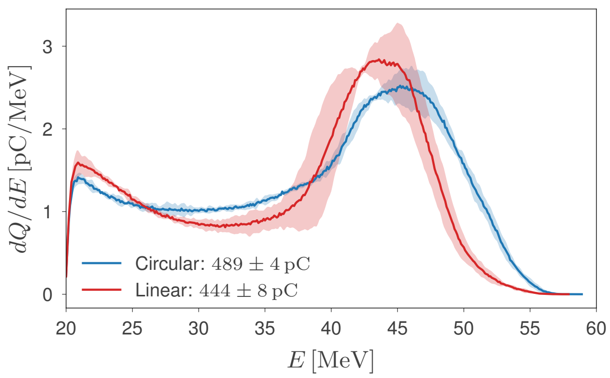


Figure 2: Electron energy spectra for the two laser polarizations. Solid lines show the mean of 3 simulations with distinct random seeds; shaded bands indicate 95% CIs. Legend keys report the mean charge and standard deviation for each case.

for the total charge, which differs by approximately 10%, both polarization states yield very similar beam properties, with minor variations in average energy, energy spread, acceleration, bunch dimensions, emittance, and divergence.

## CONCLUSION

Circular polarization increases the electron charge above 20 MeV by ~ 10%, while differences in average energy, energy spread, emittance, divergence, and other beam parameters remain within a few percent. These results suggest that laser polarization mainly influences self-injection efficiency, with little effect on beam quality. Although the values of Table 1 depend on the adopted threshold (20 MeV), its choice does not affect the high-charge bunch near 40 MeV shown in Figure 2, the most remarkable feature of the spectra. Laser-to-beam energy conversion efficiencies of 18.9% and 16.6% were achieved, for circular and linear polarizations, respectively. These values are about one order of magnitude higher than those typically reported for LWFA in gas targets.

## ACKNOWLEDGEMENTS

The authors acknowledge computing resources provided by LNCC's SDumont HPC system (project LPA-FARMA).

## REFERENCES

[1] E. Esarey, C. B. Schroeder, and W. P. Leemans, "Physics of laser-driven plasma-based electron accelerators," *Rev. Mod.*

*Phys.*, vol. 81, no. 3, pp. 1229–1285, 2009. 10.1103/RevModPhys.81.1229

[2] A. Lindstrøm, S. Corde, R. D'Arcy, *et al.* "Beam-driven plasma-wakefield acceleration," *arXiv*, pp. 2504.05558, 2025. 10.48550/arXiv.2504.05558

[3] R. D. Ruth, A. W. Chao, P. L. Morton, *et al.* "A plasma wake field accelerator," *Part. Accel.*, vol. 17 pp. 171-189, 1985.

[4] T. Tajima, and J. M. Dawson, "Laser Electron Accelerator," *Phys. Rev. Lett.*, vol. 43, no. 4, pp. 267–270, 1979. 10.1103/PhysRevLett.43.267

[5] P. Chen, J. M. Dawson, R. W. Huff, *et al.* "Acceleration of Electrons by the Interaction of a Bunched Electron Beam with a Plasma," *Phys. Rev. Lett.*, vol. 54, no. 7, pp. 693–696, 1985. 10.1103/PhysRevLett.54.693

[6] B. S. Nunes, S. P. Santos, R. P. Nunes, *et al.* "Bayesian optimization of laser wakefield acceleration in the self-modulated regime (SM-LWFA) aiming to produce molybdenum-99 via photonuclear reactions," *Phys. Plasmas*, vol. 32, no. 3, pp. 033101, 2025. 10.1063/5.0244268

[7] L. Labate, D. Palla, D. Panetta, *et al.* "Toward an effective use of laser-driven very high energy electrons for radiotherapy: Feasibility assessment of multi-field and intensity modulation irradiation schemes," *Sci. Rep.*, vol. 10, no. 1, pp. 17307, 2020. 10.1038/s41598-020-74256-w

[8] R. W. Assmann, M. K. Weikum, T. Akhter, *et al.* "EuPRAXIA Conceptual Design Report," *Eur. Phys. J. Spec. Top.*, vol. 229, no. 24, pp. 3675–4284, 2020. 10.1140/epjst/e2020-000127-8

[9] C. B. Schroeder, E. Esarey, C. G. R. Geddes, *et al.* "Physics considerations for laser-plasma linear colliders," *Phys. Rev. ST Accel. Beams*, vol. 13, no. 10, pp. 101301, 2010. 10.1103/PhysRevSTAB.13.101301

[10] C. B. Schroeder, C. Benedetti, E. Esarey, *et al.* "Laser-plasma-based linear collider using hollow plasma channels," *Nucl. Instrum. Methods Phys. Res., Sect. A*, vol. 829, pp. 113–116, 2016. 10.1016/j.nima.2016.03.001

[11] C. Bonţoiu, Ö. Apsimon, E. Kukstas, *et al.* "Author Correction: TeV/m catapult acceleration of electrons in graphene layers," *Sci. Rep.*, vol. 13, pp. 2845, 2023. 10.1038/s41598-023-29761-z

[12] C. Bonţoiu, A. Bonatto, Ö. Apsimon, *et al.* "Numerical study of self-injected electron acceleration in CNT structured targets driven by an 800 nm laser," *Sci. Rep.*, vol. 15, no. 1, pp. 45323, 2025. 10.1038/s41598-025-29386-4

[13] H. Burau, R. Widera, W. Hönig, *et al.* "PIConGPU: A Fully Relativistic Particle-in-Cell Code for a GPU Cluster," *IEEE T. Plasma Sci.*, vol. 38, no. 10, pp. 2831-2839, 2010. 10.1109/TPS.2010.2064310

[14] J.-L. Vay, M. Acciarri, A. Almgren, *et al.* "BLAST-WarpX/warpx: 26.02 (26.02)" *Zenodo*, 2026. 10.5281/zenodo.18475787

[15] C. F. R. Caron and R. M. Potvliege, "Free-space propagation of ultrashort pulses: Space-time couplings in Gaussian pulse beams," *J. Mod. Opt.*, vol. 46, no. 13, pp. 1881–1891, 1999. 10.1080/09500349908231378

[16] A. Bonatto, G. Xia, O. Apsimon, *et al.* "Exploring ultra-high-intensity wakefields in carbon nanotube arrays: An effective plasma-density approach," *Phys. Plasmas*, vol. 30, no. 3, pp. 033105, 2023. 10.1063/5.0134960

[17] S. Gessner, E. Adli, J. M. Allen, *et al.* "Demonstration of a positron beam-driven hollow channel plasma wakefield accelerator," *Nat. Commun.*, vol. 7, no. 1, pp. 11785, 2016. 10.1038/ncomms11785